Article

Part Tailoring in Metal-Additive Manufacturing: A Step towards Functionally Graded Customized Stainless-Steel Components Using Laser Powder Bed Fusion

Ahmed Elkaseer [1,2,3,*] , Amal Charles [1,*] , Stella Schneider [1] and Steffen G. Scholz [1,2,4]

1 Institute for Automation and Applied Informatics (IAI), Karlsruhe Institute of Technology (KIT), 76344 Eggenstein-Leopoldshafen, Germany; scst1085@h-ka.de (S.S.); steffen.scholz@kit.edu (S.G.S.)
2 Karlsruhe Nano Micro Facility, Karlsruhe Institute of Technology, 76344 Eggenstein-Leopoldshafen, Germany
3 Faculty of Engineering, Port Said University, Port Fuad 42526, Egypt
4 School of Mechanical Engineering (SMEC), Vellore Institute of Technology (VIT), Vellore 632014, India
* Correspondence: ahmed.elkaseer@kit.edu (A.E.); amal.charles@kit.edu (A.C.); Tel.: +49-721-608-25754 (A.E.)

Featured Application: The work reported in this article leads towards the potential development of functionally graded structures and components using laser powder bed fusion.

Abstract: The aim of this project is to demonstrate a proof of concept by using Additive Manufacturing (AM) technology in order to demonstrate its viability for the production of tailor-made components with regions of varying (higher and lower) hardness and surface roughness within a single part. In order to do this, first a test piece is designed and printed following a full factorial design of the experiment with eight runs with varying process parameters set within different regions of one part. The structure is printed several times with the laser-powder-bed-fusion-based metal-additive-manufacturing system "Sodick LPM 325" using AISI 420 in order to test and validate the change in the achievable mechanical property and surface roughness. The above-mentioned quality marks are characterized using a tactile profilometer, Rockwell test and part density, and the results are statistically analyzed using MATLAB. The results show that the linear energy density plays a significant role in controlling the surface roughness of the top surface of the components while the hardness on the top surface is unaffected. On the side surfaces, it is known that the layer thickness plays a significant role on the surface roughness as well as hardness. Looking at the results obtained, it is seen that the variation in the obtained side surface roughness is not significant to changes in the Linear Energy Density (LED) as the layer thickness was kept constant, with only slight reductions in hardness seen. The annealing process resulted in a significant reduction in hardness. This work has shown that through the careful tailoring of processing conditions, multi-functionality within one part can be integrated and has created promising avenues for further research into achieving fully functionally graded structures.

Keywords: laser powder bed fusion; AISI 420; functional grading; tailored mechanical properties; hardness; surface roughness; additive manufacturing

1. Introduction

Metal-additive manufacturing (MAM) has established itself as a new manufacturing method for light, complex and customized parts in the automotive, aerospace and medical sectors due to its design freedom and short throughput time. As one of the most common industrial AM techniques, laser powder bed fusion (LPBF) is an MAM technology based on the powder-bed-fusion (PBF) process. In this process, a thin layer of powder, in this case metal powder, is spread onto the build platform by a recoater arm, and then selectively melted by a laser, whereupon it fuses with surrounding powder particles as well as the previous layer and builds up on the part. After the layer is finished, the platform moves

downwards, is recoated again and the process is repeated [1] (as seen in Figure 1). The process and its outcomes such as printing time, part quality and material properties depend on printing parameters such as laser power, scan speed, scan spacing, layer thickness and laser spot size [2].
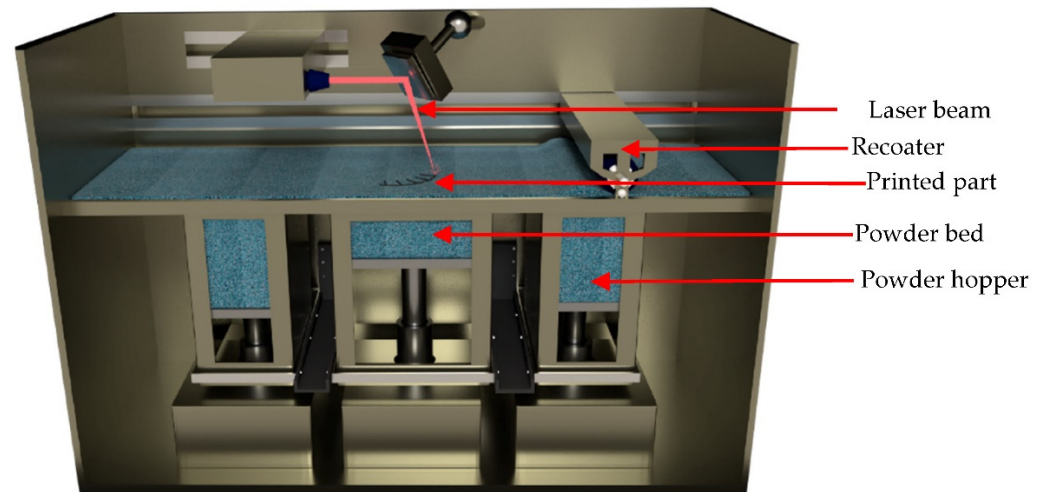

Figure 1. Visualization of the LPBF Technology.

Since the parts are built on a base plate, which is attached to the platform, post-processing steps are necessary to remove the built part from the base plate, e.g., with wire EDM [3]. Further post-processing might include a heat treatment to strengthen the mechanical properties and for the removal of residual stresses that might induce warpages and distortion in the parts, or a surface treatment such as polishing or cutting, to reduce surface roughness and to improve the overall surface finish [4].

The part quality of AM parts, regarding surface roughness and mechanical properties, is still a challenging issue to be addressed since the as-built quality is still not comparable to those produced by conventional subtractive manufacturing methods [5]. Therefore, post processing is often necessary, which diminishes the advantage of shorter production time and the design freedom offered [6,7]. Delgado et al. [8] investigated the correlation of different process parameters, such as scan speed, layer thickness and build direction, with surface roughness and macrohardness (HB) of iron-based LPBF-manufactured parts. It was found that the build direction and layer thickness have a noticeable correlation with the mechanical properties such as bending strength and elongation with no effect on tensile strength. Wang D. et al. [9] examined the effect of laser energy density E, which is influenced by laser power, scan speed and hatch spacing, on the relative density and surface roughness (microstructure) of LPBF-fabricated parts. A total of 32 cuboids with different sets of the above-mentioned parameters were printed and investigated, resulting in a range of investigated energy densities of 48–208 J/mm^3. It was found that energy density has a significant effect on surface roughness and can be divided into four different value ranges, which affect the outcome. In particular, these are the "insufficient melting zone" (E < 75 J/mm^3), the "partially balling zone" (75 J/mm^3 < E < 120 J/mm^3), the "successful fabricating zone" (120 J/mm^3 < E < 170 J/mm^3) and the "excessive melting zone" (E > 180 J/mm^3). In a following paper, Wang D. et al. [10] enlarged their study on surface morphology by concentrating on varying laser power (100–500 W) and scan speed (600–1600 mm/s) and keeping hatch spacing constant at 0.08 μm. As a result, they added another zone between the "successful fabricating zone" and the "excessive melting zone", the "smooth forming zone", and specified the parameter values for each zone, such as laser power (150 W) and scan speed (800 mm/s) for the "successful fabricating zone". Wang L. et al. [11] also looked into the effect of laser energy density on surface roughness and microhardness (HV) of selective laser-melted 30CrMnSiA steel parts by modifying the laser power and exposure time. The

experiment displayed a maximum hardness at 48.72 J/mm^3 E, above which the hardness decreased. For surface roughness, a vice versa trend was found, leading to the conclusion of an optimal laser energy density of 46.15–51.28 J/mm^3. Majeed et al. [12] studied the surface quality of AlSi10Mg LPBF-manufactured parts by evaluating the influence of laser power, scan speed, overlap rate and hatch distance. The results showed that low laser power leads to a smoother surface. Moreover, if high laser power is combined with wide hatch distances, then surface roughness increases, indicating a positive correlation. Finally, optimized values for minimum surface roughness were obtained, in particular 0.32 W laser power, 0.60 m/s scan speed and 88.7 μm hatch distance.

Some engineering components must possess multiple mechanical properties at different locations in order to fulfil their functionality. Crankshafts, for example, should have higher hardness on their outer surface than in the internal layers to withstand higher and different dynamic loads and stresses. This is usually achieved using processes such as case hardening where the outer layer of the material is exceedingly hardened using conventional case-hardening/treatment techniques. However, due to the thermal nature of the case-hardening process, it is not easy to control the thickness of the layer to be hardened. The AM of functionally graded structures is a popular research topic since AM might provide a precise alternative to unpredictable processes such as case hardening. Niendorf et al. attempted the printing of functionally graded materials using LPBF and reported that varying process parameters can create a steep microstructural gradient resulting in distinct local mechanical properties [13]. Zou et al. successfully demonstrated that by controlling the process parameters it is possible to control the grain orientation of parts printed using LPBF, thereby achieving tailored magnetic properties in Ni–Fe-based soft magnets [14]. Sridharan et al. successfully demonstrated that using MAM with steel, it is possible to fabricate components with pre-defined spatial hierarchies that emulate natural bio-inspired structures that provide components with multi-functionality [15].

It can be seen that the layer-wise nature of AM allows the production of parts with customized shapes and functionalities, which enables the integration of multi-mechanical properties in one part. In this context, the aim of this study is to examine the effect of different process parameters, namely scan speed, hatch spacing and laser power, on the output variables of surface roughness and microhardness and compare it to the standard set of parameters, and thus to demonstrate the potential to precisely tailor these parameters to the desired process outcome and produce parts with multi-functionality of varying hardness and surface roughness within a single part.

2. Materials and Methods

2.1. Design of Experiments

In order to enable the testing of the tailoring of properties so as to instill different surface textures and mechanical properties within one part, one cuboid with the dimensions of 15.5 × 15 × 30 mm (H × W × D) was printed as seen in Figure 2. An additional 0.5 mm was added to the height in order to compensate for the height loss when the parts were removed from a base plate by wire cutting. The parameters were set in such a way as to create two equal distinct volumes within the cuboid that were printed with different parameter settings. This is also seen in Figure 2, where the parameter settings of the half colored in red were kept constant with standard processing parameters, and the settings of the blue cuboidal volume were varied according to a Design of Experiments (DoE).

The factors of scan speed (*v*), hatch spacing (*h*) and laser power (*P*) were varied at two levels, whereas the layer thickness (t) was kept constant. The linear energy density was also calculated as seen in Equation (1), as it allowed an understanding of the melt-pool level dynamics involved.

$$E = \frac{P}{v} \tag{1}$$

A design of experiments was performed, where the red cuboid represents the standard printing settings and serves as the reference data (*v* = 1200 mm/s, *h* = 0.08 mm, *P* = 400 W),

whereas the settings of the blue cuboid were changed following a full factorial plan with eight runs (see Figure 2).
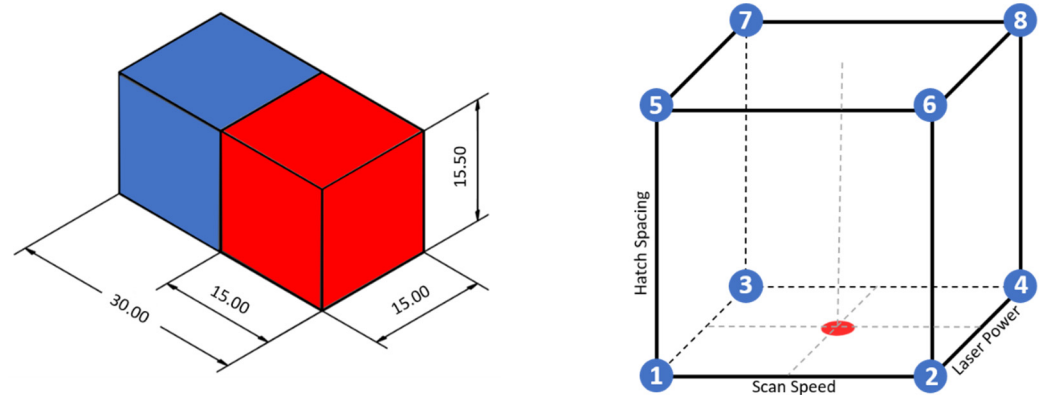

Figure 2. Test structure and respective CCD (all dimensions are in mm).

The values for the DoE were chosen based on previous experience with the LPBF system and represent values adjacent to the standard processing parameters as suggested by the machine manufacturer. Basically, one level value for the DoE was chosen below the standard setting and one above it, except for the hatch-spacing values, since due to limitations in the printer settings, only two hatch-spacing values were adjustable (as seen in Table 1).

Table 1. Applied Design of Experiment.

Run	Scan Speed (v)	Hatch Spacing (h)	Laser Power (P)	Linear Energy Density (E)
	[mm/s]	[mm]	[W]	[J/mm]
1	900	0.08	350	0.39
2	1500	0.08	350	0.23
3	900	0.08	450	0.50
4	1500	0.08	450	0.30
5	900	0.12	350	0.39
6	1500	0.12	350	0.23
7	900	0.12	450	0.50
8	1500	0.12	450	0.30
9 (Ref)	1200	0.08	400	0.33

The regression analysis was performed with MATLAB (R2019a) and only the obtained data from the blue cuboid was used. The measured values of the standard printed cuboid were used as reference values to determine the impact of the process parameters differing from the recommended standard settings.

2.2. Printing Process

For each run, a set of four samples was printed with the 3D MAM system "Sodick LPM 325" (see printed samples in Figure 3). Using the software "LS-Beams" the printing process parameters were set. For all the samples, a layer thickness of 50 μm and the scanning pattern visualized in Figure 4 was applied. It was a rectangular cell pattern where the contour was scanned first and then the inside. The printer was equipped with an Yb-fiber laser with a wavelength of 1070 nm. The material used for printing was recycled AISI 420 with a particle size of 25–45 μm.
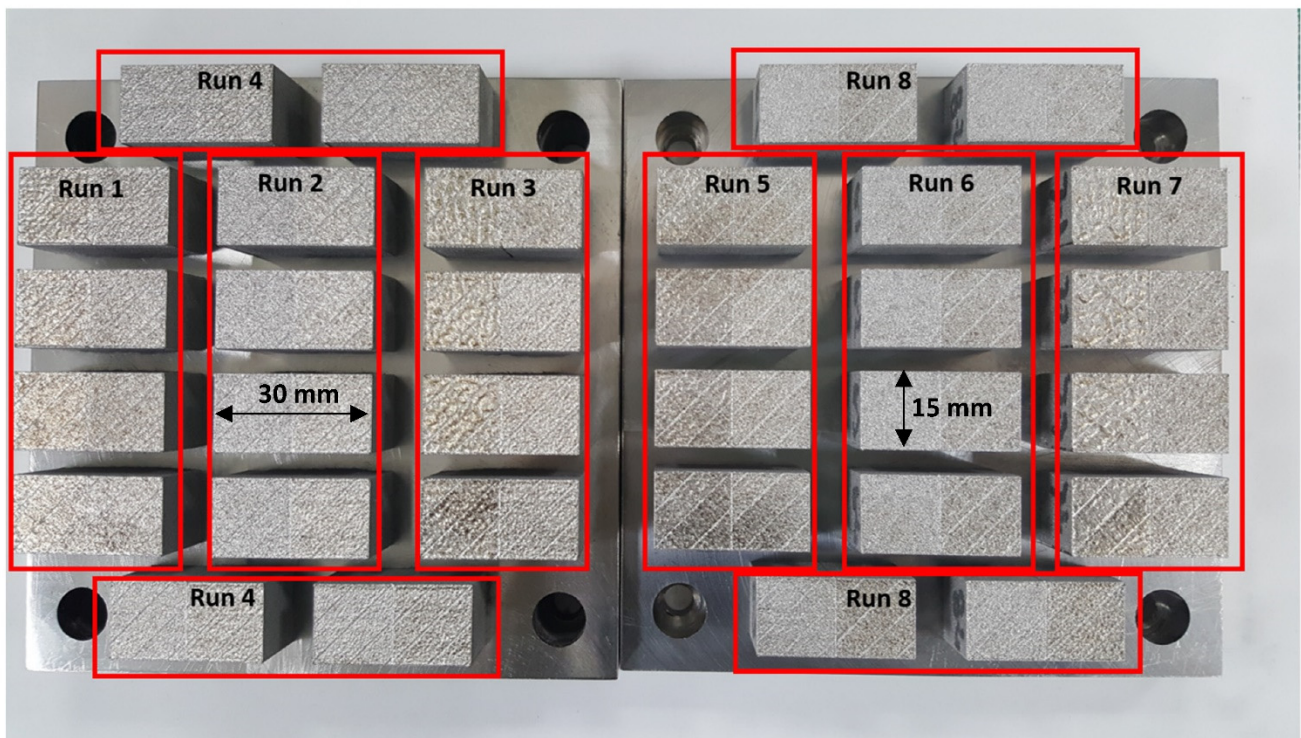
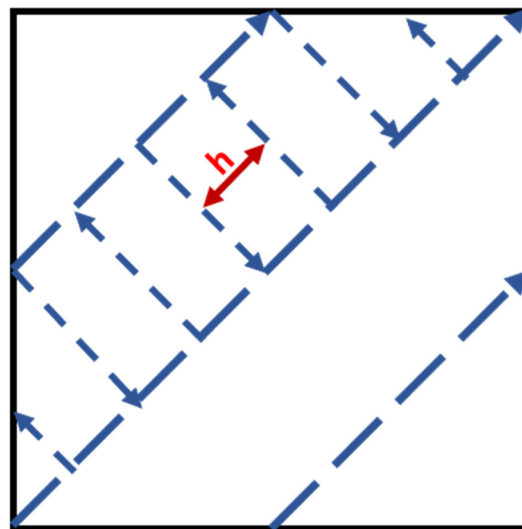**Figure 3.** Component layout on base plate.

Figure 4. Applied laser-scanning pattern.

2.3. Characterization

2.3.1. Surface Roughness

To investigate the surface roughness, the arithmetical mean roughness R_a (see Equation (2) [16]) was measured with a tactile profilometer (Mitutoyo SJ-410) according to ISO 4287–1997 [17], with an expected roughness around 10 μm resulting in a measuring length of 12.5 mm.

$$R_a = \frac{1}{l} \int_0^l |z| \, dz \tag{2}$$

Hence, for each sample, the top perpendicular to the longer edge of the sample and the front-facing side perpendicular to the layers were assessed (see Figure 5).
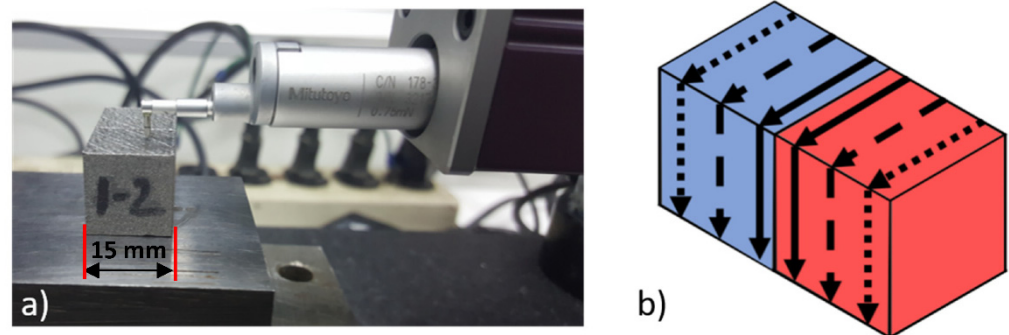
Figure 5. (**a**) Tactile profilometer "Mitutoyo SJ-410"; (**b**) illustration of measurement direction.

2.3.2. Hardness

In order to measure the hardness, it was necessary to prepare the samples through grinding and polishing. Again, the top and front-facing sides were assessed, though only one sample was investigated using the "Future Tech–Rockwell Hardness Tester FR" (as seen in Figure 6).
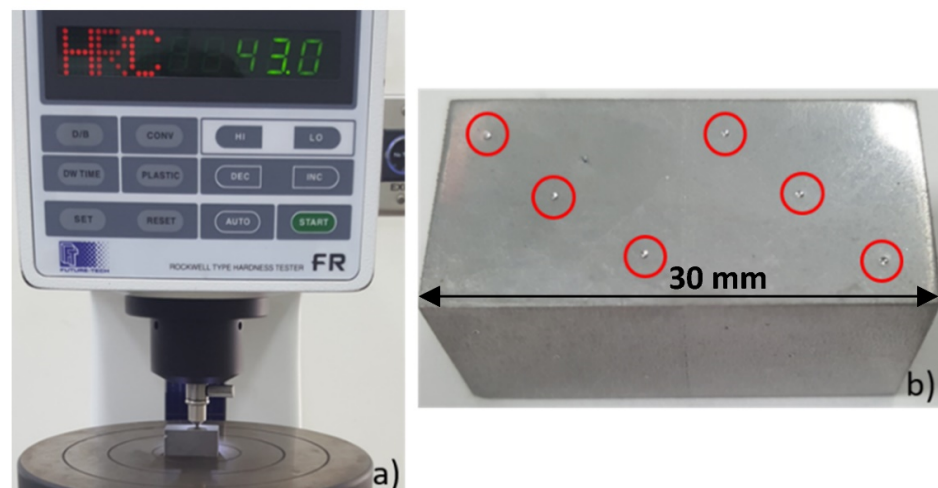

Figure 6. (**a**) Rockwell Type Hardness Tester; (**b**) illustration of measuring points.

The Rockwell hardness test uses an indenter, onto which two different forces are applied and the resulting indentation depth in the material is measured. Depending on the material and application, different forces and indenter types are used, referred to as the Rockwell hardness scale. In this study, the Rockwell hardness scale C (HRC) was applied with a diamond indenter and an initial force of 10 kgf followed by 150 kgf. The hardness number was calculated by the hardness tester following the structure of Equation (3) [18].

$$HR = 100 - \frac{d}{0.002 \text{ mm}} \tag{3}$$

2.3.3. Heat Treatment

For the heat treatment, annealing was chosen, since during the printing process a lot of internal stress arises inside the built part due to repeated heating and cooling processes. Hence, annealing is often used to release that internal stress inside MAM parts. However, an annealing heat treatment is accompanied by an unintended reduction in hardness [19]. Therefore, an investigation of the influence of annealing on the hardness affected by the chosen parameters was conducted.

The temperature development during the annealing process can be divided into three steps. First, the oven was heated up from room temperature to 650 °C over two hours.

During the next two hours, the samples were annealed at 650 °C. Within approximately 20 h the parts cooled down to room temperature.

2.3.4. Density Measurement

Selected samples of high and low LED were subjected to density measurements using the Archimedes principle. The measurements were carried out using a Sartorius YDK03 system with an accuracy scale of 0.0001 g and the measurements were made with a water temperature of 25.5 °C.

3. Results and Discussion

In this section, the effect of the process parameters and their interactions on the two output variables will be analyzed, interpreted and checked against previous studies. Furthermore, a comparison between top- and side-surface results as well as between measured values before and after the heat treatment will be drawn. Note that the results of the standard parameters are highlighted in the graphs.

3.1. Surface Roughness

In Figure 7, the measured values of the roughness R_a on all top and side samples are summarized. Overall, clear trends are visible. With an increase in the linear energy density of the top surface, the R_a decreased up to a certain point (Approx. 0.40 J/mm) before it increased once again. This can be attributed to the fact that at low LED, there is insufficient energy to achieve the complete melting of the powder particles on the top surface, which results in spatter and balling due to the unsteady melt pool. This is known to create high surface roughness [5]. The surface roughness was seen to drop when the LED increased and operated closer to a stable melt-pool condition, such as in a conduction mode [20]. A higher LED can lead to keyhole melt mode of the melt pool that can lead to further surface defects caused by the unstable melt pool [21]. While for the side surface, it can be seen that the LED did not have a significant trend and the R_a remained constant throughout with only minute variations. This could be explained by the applied layer thickness, which was the same for all samples. Hence, the roughness profile on the side is similar. Using the LED of 0.39 J/mm, a lower surface roughness was achieved on the top surface in comparison to the standard parameter within the same component.
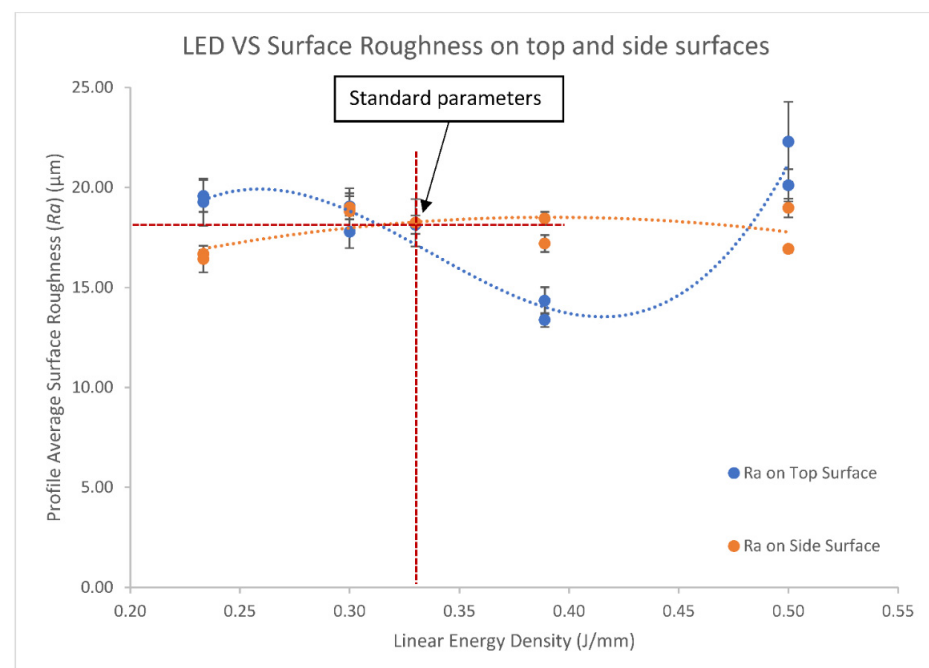

Figure 7. Measured surface roughness R_a on the top and side surface.

3.1.1. Top Surface

Looking at Figure 8, laser power had the greatest effect on the top surface roughness with increasing laser power also increasing the roughness due to the increased LED, as explained above. This result agrees with the results of the analysis of variance (ANOVA), which indicate the interaction of laser power and scan speed as the most significant (*p*-value: 0.037), followed by laser power (*p*-value: 0.044). Generally, it can be said that all three parameters increased surface roughness proportionally.
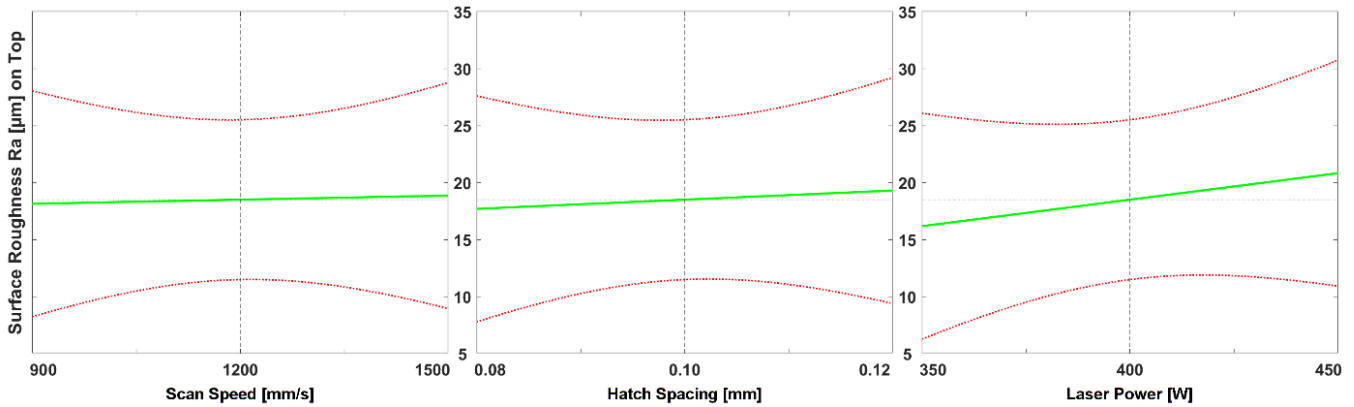
Figure 8. Predicted effects of changes in process parameters on the roughness R_a on the top surface, where the green lines are the predictions of surface roughness on top surfaces and the dotted red lines present the 95% confidence bounds.

In Figure 9, the interactions of the three parameters are displayed. Scan speed and laser power did seem to have a strong interaction effect on surface roughness, since varying them caused large variations in roughness, while hatch spacing did not seem to have a significant effect.
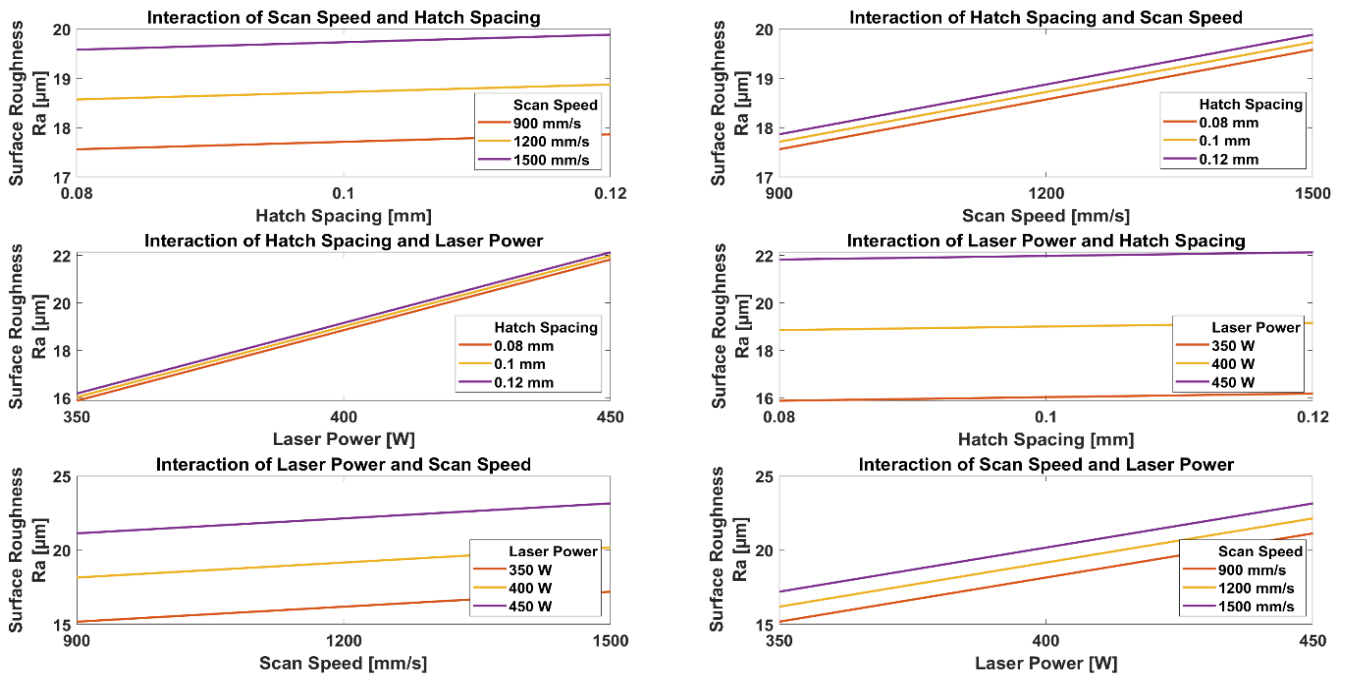

Figure 9. Effects of the interaction of parameters on the measured R_a on the top surface.

3.1.2. Side Surface

Regarding the side surface, the three chosen process parameters did not seem to have a significant influence, although a trend is recognizable in Figure 10 in all three plots. This

was verified by ANOVA, with laser power being the most influencing parameter with a *p*-value of 0.18, which was not considered as significant since it was greater than 0.05. The second- and third-most influencing aspects were the interaction of scan speed and hatch spacing (*p*-value = 0.24) and the interaction of scan speed and laser power (*p*-value = 0.28), which were also not regarded as significant. This result could be explained by the fact that the layer thickness was the same in all samples and therefore, the outer surface roughness on the side remained similar and unaffected by the different LED values.
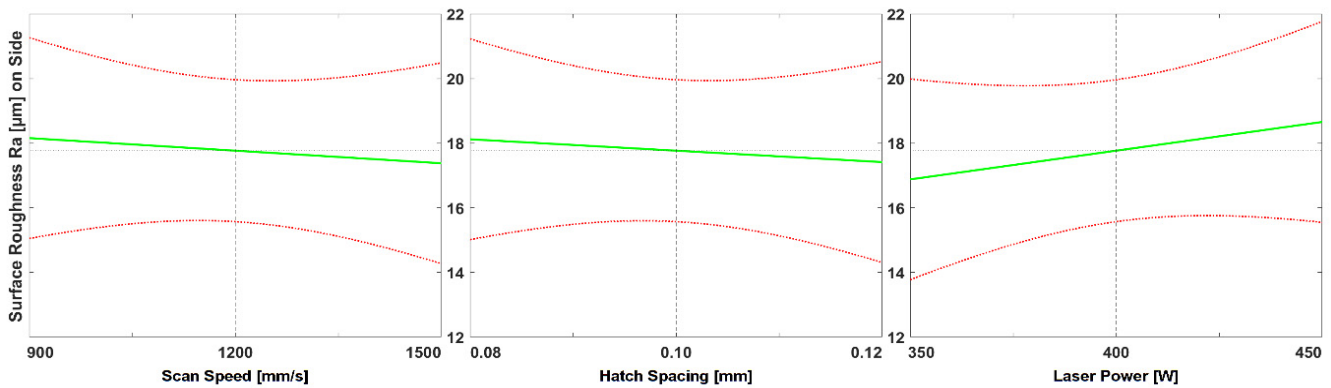
Figure 10. Predicted effects of changes in process parameters on the roughness R_a on the side surface, where the green lines are the predictions of surface roughness on side surfaces and the dotted red lines present the 95% confidence bounds.

Figure 11 displays the interaction effects of the three parameters regarding the surface roughness on the side. By comparing these to the ANOVA results, it is visible that interactions with the parameter scan speed were more influencing since the gaps between the graphs and the tilt were greater. Low scan speeds, paired with either small hatch spacing or high laser power, caused higher roughness due to the over-melting of the powder.
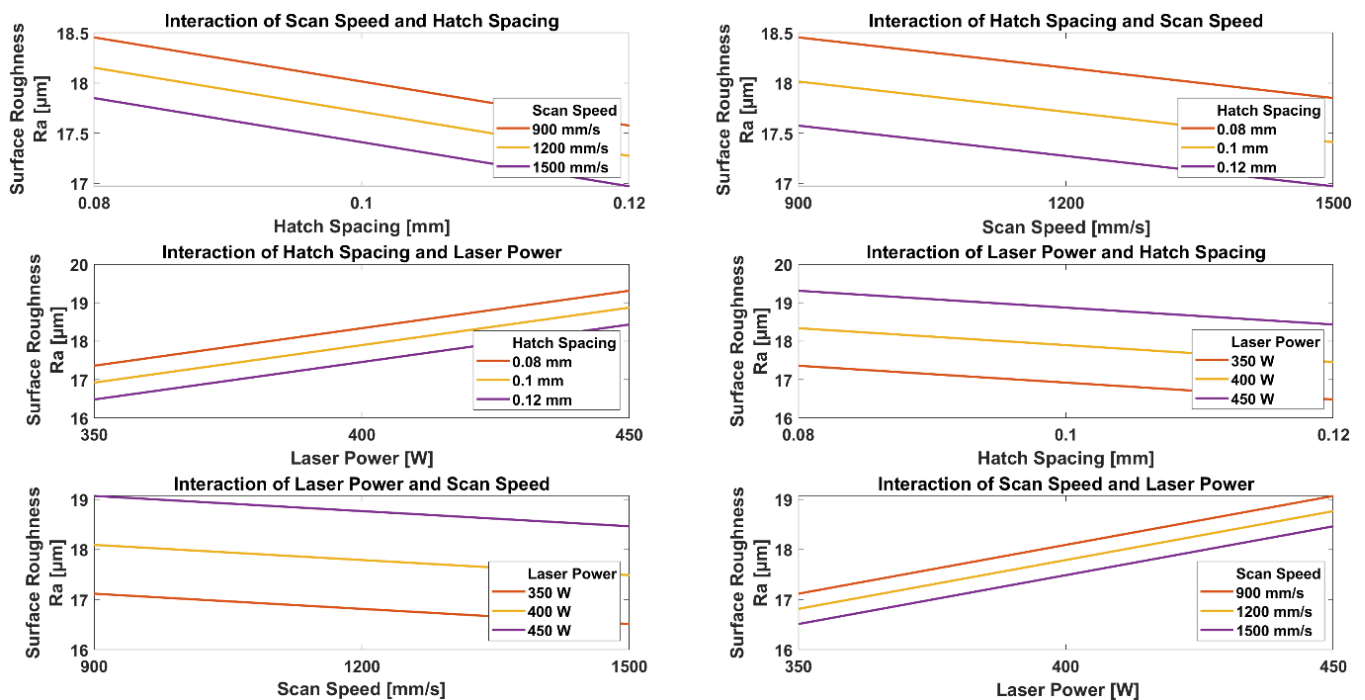

Figure 11. Effects of the interaction of parameters on the measured R_a on the side surface.

3.2. Hardness

Figure 12 illustrates the overall results of the measured Rockwell hardness on the top and side surfaces, showing an overall higher hardness on the top surface.
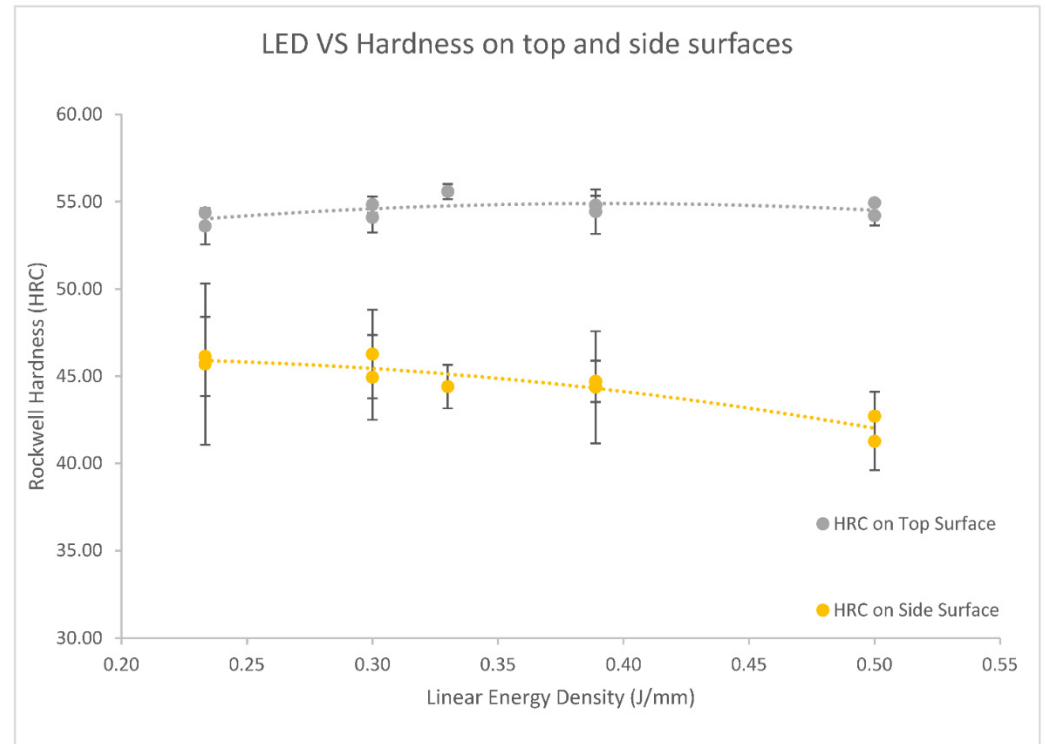

Figure 12. Measured Rockwell hardness HRC on the top and side surfaces.

Considering the range of the error bars of the values measured on the side, the results could not be regarded as solid and reliable. Therefore, no linear regression analysis was conducted for the effect of the process parameters on the hardness on the side surface. This high standard deviation of the values can be attributed to the layer profile on the side surface, meaning that due to the layer-by-layer addition of material, there can be locations on the side surface, such as the areas in between layers, where there might be pores, or the presence of unmelted powder, etc., which will affect the side hardness measurement. Therefore, during indentation, the tip might contact solid material or porous areas, which creates the large variations due to different surface conditions at the indentation points (as seen in Figure 13).
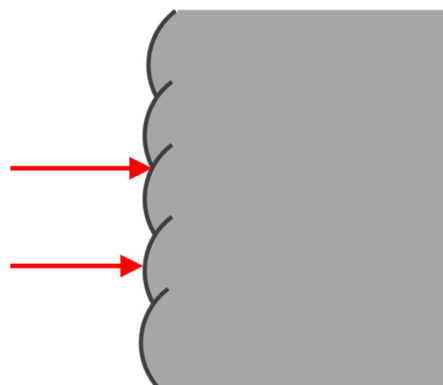

Figure 13. Possible indentation points on the side surface.

Hardness of Top Surface

As abstracted from Figure 14 and ANOVA, the three process parameters had no significant influence on the hardness of the top surface. The most important parameter obtained from ANOVA, though not significant, was the scan speed with a *p*-value of 0.579.
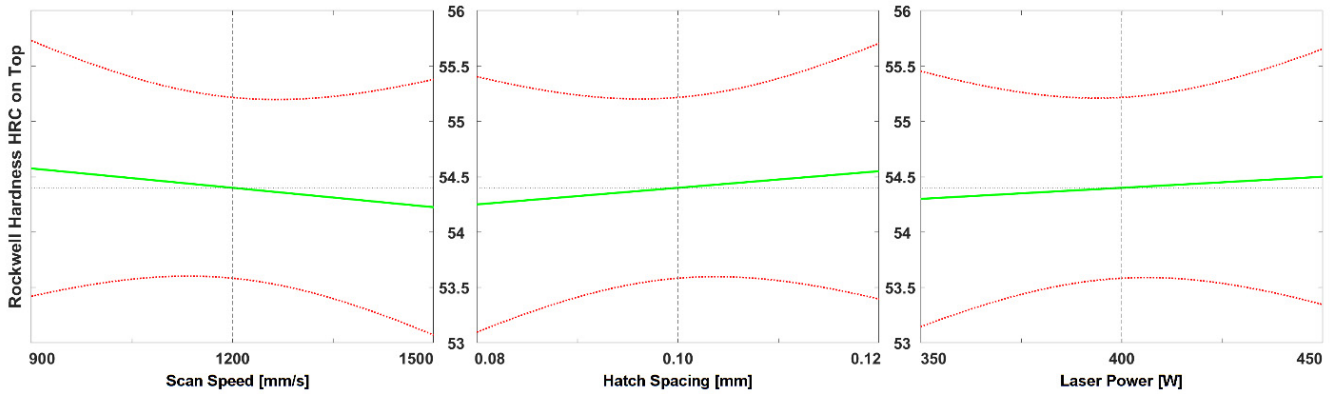

Figure 14. Predicted effects of changes in process parameters on the Rockwell hardness HRC on the top surface, where the green lines are the predictions of hardness on top surfaces and the dotted red lines present the 95% confidence bounds.

Additionally, the interaction plots illustrated in Figure 15 show no clear interaction effects between the parameters. Only the effects of laser power and hatch spacing are more distinctive, which was validated by being the second-most important term in ANOVA (*p*-value = 0.626). It can be said that when applying small hatch-spacing values, the laser power can make a small difference regarding the hardness. The effect of scan speed at certain laser powers causes slight deviations in hardness.
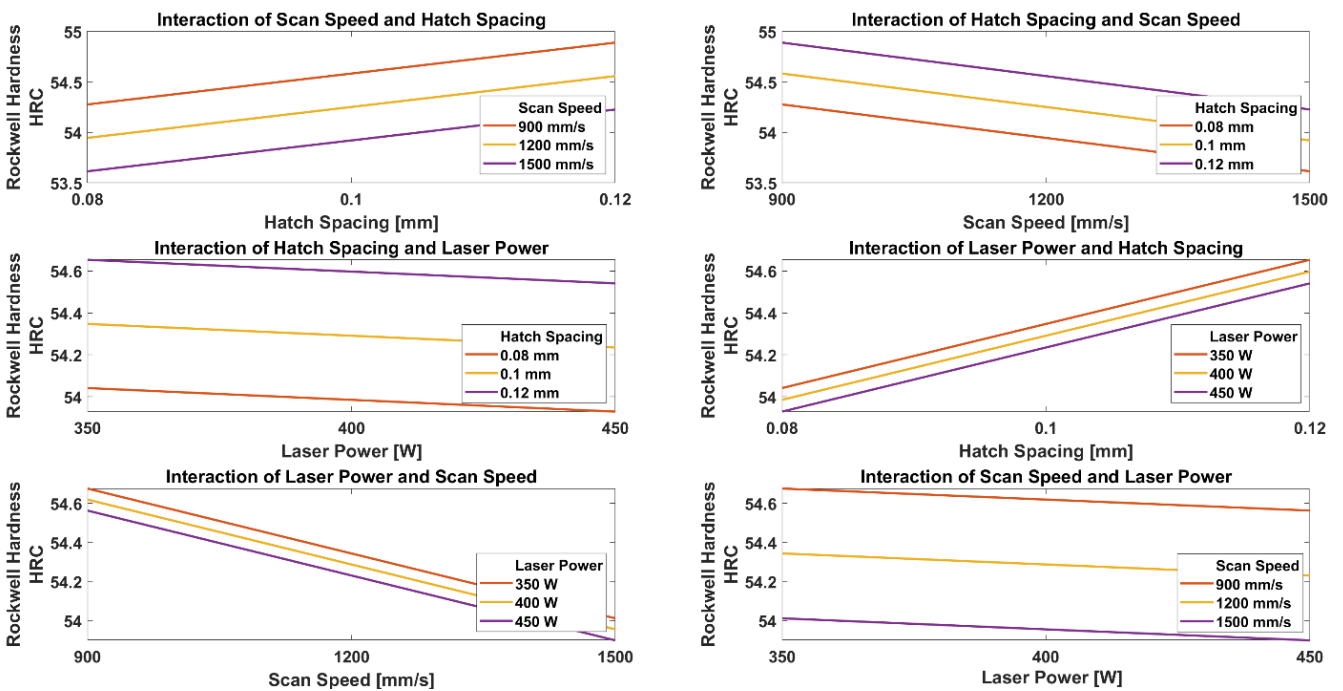

Figure 15. Effects of the interaction of parameters on the measured HRC on the top surface.

3.3. Effect of Annealing

The effect of annealing on the hardness is clearly detectable in Figures 16 and 17. The hardness was reduced by approximately 40% on the top and 50% on the side. The decrease

in hardness can be attributed to a reduction in internal stress through annealing; however, the trend of the reduced hardness due to the annealing step remained consistent on both the top and side surfaces.
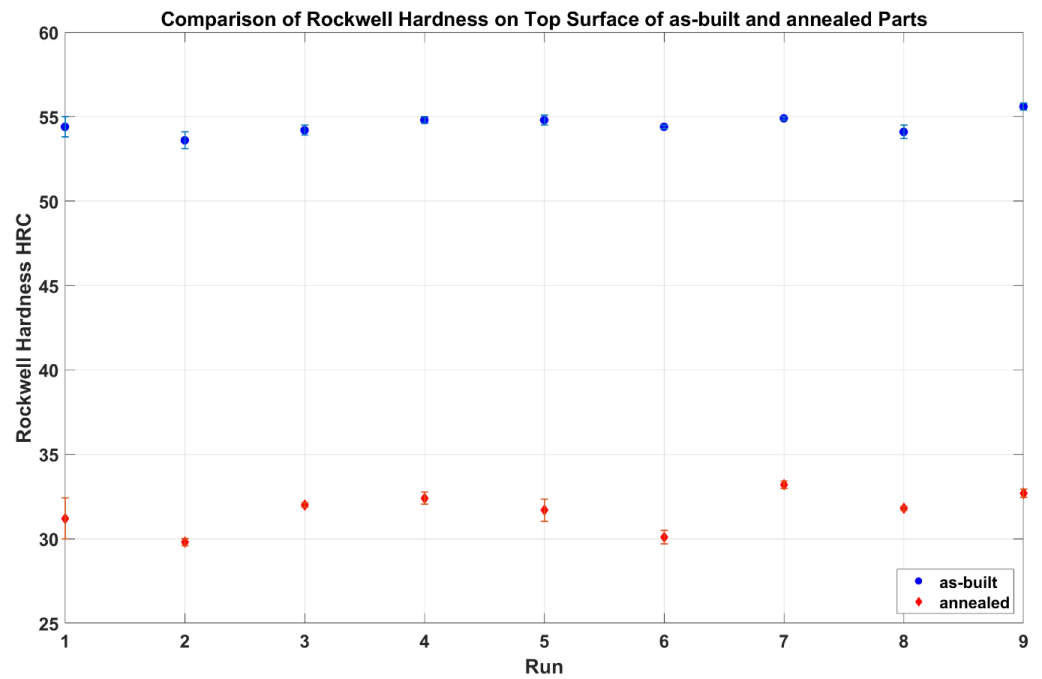

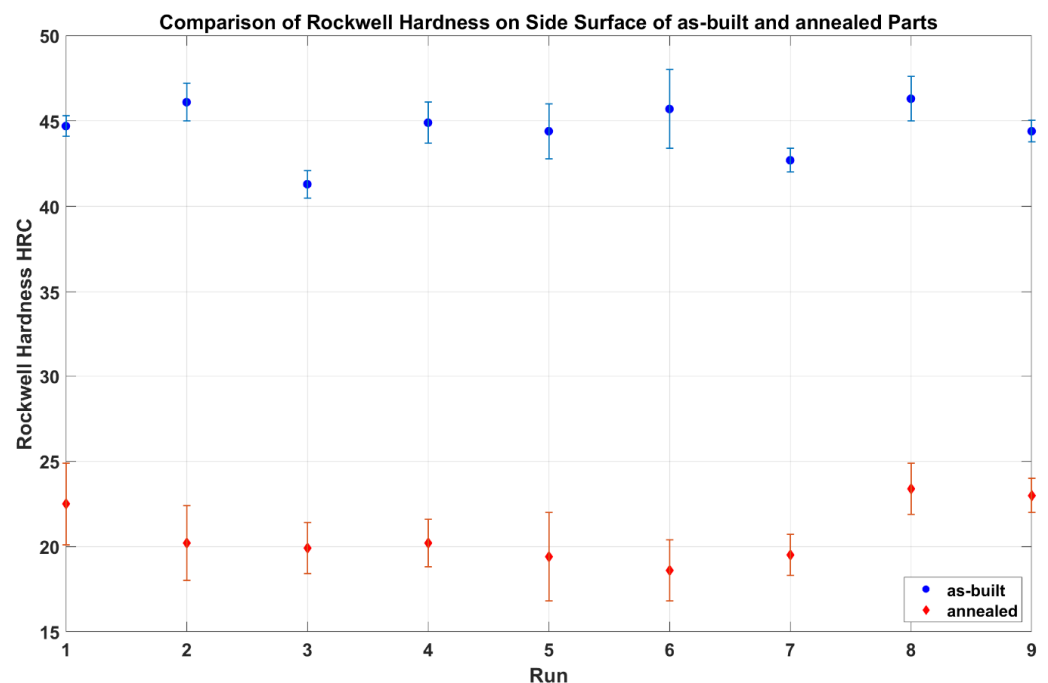**Figure 16.** Effect of annealing on Rockwell hardness HRC on the top surface.

Figure 17. Effect of annealing on Rockwell hardness HRC on the side surface.

3.4. Microscopic Analysis

Microscopic images of the top surface along with 3D height maps of various samples produced with different laser energy densities can be seen in Figure 18 and Figure 19, respectively. These images allow us to explain various aspects that resulted in the observed and measured surface roughness and hardness.
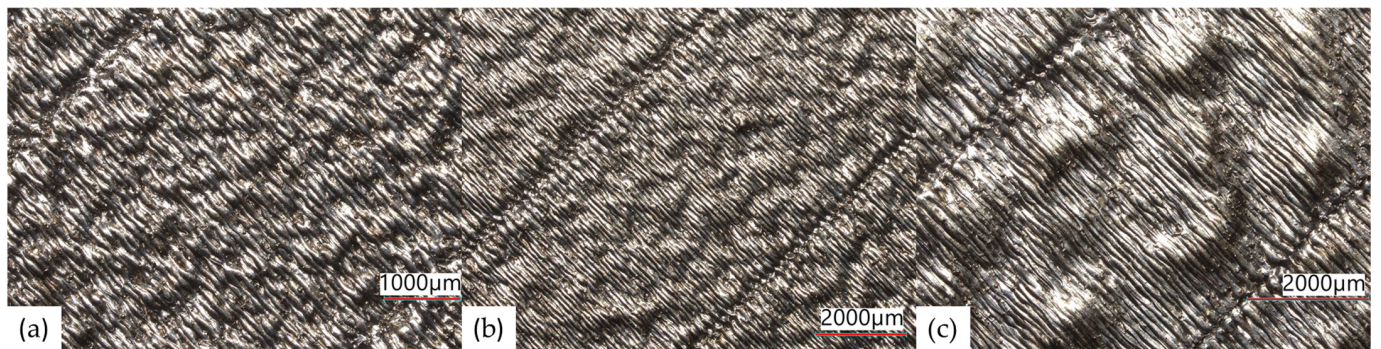
Figure 18. Top surface of (**a**) low-LED test piece (0.23 J/mm), (**b**) reference LED test piece (0.33 J/mm) and (**c**) high-LED test piece (0.50 J/mm).
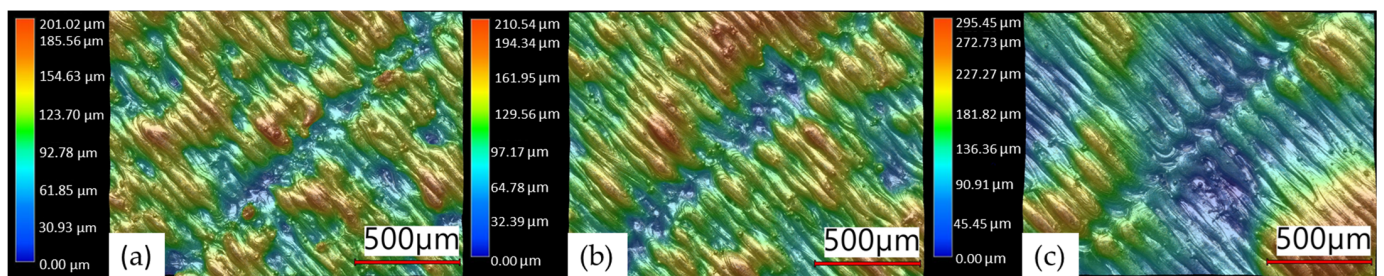

Figure 19. 3D Height maps of (**a**) low-LED test piece (0.23 J/mm), (**b**) reference LED test piece (0.33 J/mm) and (**c**) high-LED test piece (0.50 J/mm).

When looking at the surfaces seen in Figure 18, it is clear that the surface of the samples produced with low LED, as in Figure 18a, exhibits a high surface roughness, as there are a lot of randomized asperities that cause an uneven surface texture, which is responsible for the high average surface roughness. The surface in Figure 18b displays more regularity and therefore a slightly lower measured surface roughness, while Figure 18c is of a surface that displays large wavy topography and large depressions and peaks at the border of scan tracks, which are also responsible for the increased surface roughness. Figure 19 goes on to support these claims; it can be seen that major depressions are formed on the surface at the locations where scan vectors change direction, namely at the border of the scanning cell. From Figure 19a,b, it is clear that that this depression is smaller when printing with a lower LED, as the melt pools formed are smaller and do not have large drilling effects on the surface. However, as can be seen in Figure 19c, when printing with a larger LED, the melt pool, especially at the edge of the scan vectors, can transition into the keyhole mode, which results in larger drilling into the surface, which agrees with what was reported in [21]. This also results in a higher surface roughness and possibly in the incidence of keyhole-induced porosity.

Figure 20 shows microscopic images of the polished surfaces, which can provide a better idea of the surface integrity that can affect the hardness. Figure 20a shows a surface that manifested with a large number of porosities and a lack of fusion defects that were caused due to insufficient melting energy absorbed from the laser. This increased porosity was responsible for the marginally decreased hardness of the low-LED sample. In Figure 20b, we see the absence of surface defects, which explains the higher hardness of this surface, and Figure 20c also shows the absence of any major porosity, which explains the slightly higher measured hardness of the sample. Minor defects may have manifested in the form of keyhole-induced porosity [21].
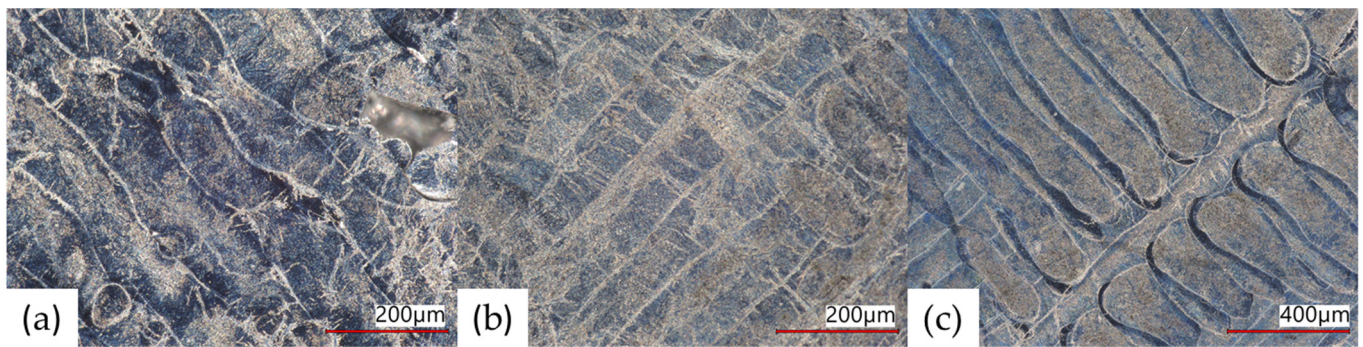
Figure 20. Microscopic images of the polished surfaces of (**a**) low LED test piece (0.23 J/mm), (**b**) Reference LED test piece (0.33 J/mm) and (**c**) high LED test piece (0.50 J/mm).

The observations made above were confirmed using density measurements made by employing the Archimedes principle. Noting that annealed grade AISI 420 has a density of 7.800 g/cm^3, the measured density for the low-LED (0.23 J/mm) sample was 7.668 g/cm^3, which indicates the presence of a higher amount of porosity within the volume of the sample according to the explanations provided above, such as due to a lack of fusion pores. This increased porosity of the lower-LED samples was also responsible for the lower measured hardness.

The high-LED (50 J/mm) sample exhibited an average density of 7.715 g/cm^3, which points towards the presence of lower porosity in the sample. This is also in accordance with the explanations provided above, where the reduced density may have been caused by the presence of a small number of keyhole pores. The increased density contributed to the higher hardness when compared to the lower-LED samples.

4. Conclusions and Outlook

This study experimentally investigated the influence of applying different printing process parameters within the bulk of the same part in order to induce and tailor surface as well as mechanical properties within one component. To achieve this, surface roughness and hardness measurements were systematically acquired by conducting a DoE and regression analysis. After evaluating the results, it can be said that the most important parameters were laser power, scan speed, and their interaction, which led to the creation of parts with different functional performances at different locations. The following are specific conclusions that can be made:

1. The linear energy density applied by the laser played a major role in the top surface roughness with high surface roughness seen in low energy densities, caused by insufficient melting. The surface roughness decreased as a more stable melt pool was reached when the LED increased. However, after a point, the surface roughness increased once again due to other printing defects that manifested due to the high LED.
2. Surface roughness on the side surfaces was seen to be consistent as they were mostly affected by the chosen layer thickness, which was kept constant for all the trials.
3. The hardness on the side surface was highly unpredictable due to the unstable nature of measuring the hardness created due to the layers.
4. For the hardness on the top surface, the hardness remained consistent for the various LEDs tested, with the scan speed seen as the most influential parameter.
5. Low-LED samples had lower density than the higher-LED samples, which was consistent with the resultant hardness.

This research work has proven to be a step towards integrating multi-functionality and functionally graded materials within one part through gradually tuning the process parameters across a component. In order to obtain a deeper understanding of said topic, it could also be helpful to investigate the microstructure of the parts and shed some light on the grain structure and size, which will be the topic of future studies.

References

1. Yang, L.; Hsu, K.; Baughman, B.; Godfrey, D.; Medina, F.; Menon, M.; Wiener, S. *Additive Manufacturing of Metals: The Technology, Materials, Design and Production*; Springer Series in Advanced Manufacturing; Pham, D.T., Ed.; Springer: Berlin/Heidelberg, Germany, 2017.
2. Diegel, O.; Nordin, A.; Motte, D. *A Practical Guide to Design for Additive Manufacturing*; Springer Series in Advanced Manufacturing; Pham, D.T., Ed.; Springer: Singapore, 2019.
3. Gibson, I.; Rosen, D.; Stucker, B. *Additive Manufacturing Technologies—3D Printing, Rapid Prototyping, and Direct Digital Manufacturing*, 2nd ed.; Springer: New York, NY, USA, 2015.
4. Gebhardt, A.; Hötter, J. *Additive Manufacturing 3D Printing for Prototyping and Manufacturing*; Carl Hanser Verlag: Munich, Germany, 2016.
5. Charles, A.; Elkaseer, A.; Thijs, L.; Hagenmeyer, V.; Scholz, S. Effect of Process Parameters on the Generated Surface Roughness of Down-Facing Surfaces in Selective Laser Melting. *Appl. Sci.* **2019**, *9*, 1256. [CrossRef]
6. Bikas, H.; Stavropoulos, P.; Chryssolouris, G. Additive manufacturing methods and modelling approaches: A critical review. *Int. J. Adv. Manuf. Technol.* **2016**, *83*, 389–405. [CrossRef]
7. Gardan, J. Additive manufacturing technologies: State of the art and trends. *Int. J. Prod. Res.* **2016**, *54*, 3118–3132. [CrossRef]
8. Delgado, J.; Ciurana, J.; Rodríguez, C.A. Influence of process parameters on part quality and mechanical properties for DMLS and SLM with iron-based materials. *Int. J. Adv. Manuf. Technol.* **2012**, *60*, 601–610. [CrossRef]
9. Wang, D.; Liu, Y.; Yang, Y.; Xiao, D. Theoretical and experimental study on surface roughness of 316L stainless steel metal parts obtained through selective laser melting. *Rapid Prototyp. J.* **2016**, *22*, 706–716. [CrossRef]
10. Wang, D.; Dou, W.; Yang, Y. Research on Selective Laser Melting of Ti6Al4V: Surface Morphologies, Optimized Processing Zone, and Ductility Improvement Mechanism. *Metals* **2018**, *8*, 471. [CrossRef]
11. Wang, L.-Z.; Wei, W.-H. Selective Laser Melting of 30CrMnSiA Steel: Laser Energy Density Dependence of Microstructural and Mechanical Properties. *Acta Metall. Sin. (Engl. Lett.)* **2018**, *31*, 807–814. [CrossRef]
12. Majeed, A.; Ahmed, A.; Salam, A.; ZakirSheikh, M. Surface quality improvement by parameters analysis, optimization and heat treatment of AlSi10Mg parts manufactured by SLM additive manufacturing. *Int. J. Lightweight Mater. Manuf.* **2019**, *2*, 288–295. [CrossRef]
13. Niendorf, T.; Leuders, S.; Riemer, A.; Brenne, F.; Tröster, T.; Richard, H.A.; Schwarze, D. Functionally Graded Alloys Obtained by Additive Manufacturing. *Adv. Eng. Mater.* **2014**, *16*, 857–861. [CrossRef]
14. Zou, J.; Gaber, Y.; Voulazeris, G.; Li, S.; Vazquez, L.; Liu, L.-F.; Yao, M.-Y.; Wang, Y.-J.; Holynski, M.; Bongs, K.; et al. Controlling the grain orientation during laser powder bed fusion to tailor the magnetic characteristics in a Ni-Fe based soft magnet. *Acta Mater.* **2018**, *158*, 230–238. [CrossRef]
15. Sridharan, N.; Gussev, M.; Babu, S. Tailoring plasticity mechanisms in compositionally graded hierarchical steels fabricated using additive manufacturing. *Sci. Rep.* **2021**, *11*, 20112. [CrossRef] [PubMed]
16. Thomas, T.R. Characterization of surface roughness. *Precis. Eng.* **1981**, *3*, 97–104. [CrossRef]
17. ISO/ASTM. *Geometrical Product Specification—Surface Texture: Profile Method—Terms Definitions and Surface Texture Parameters*; International Organization for Standardization: London, UK, 1997.

18.   Low, S.R. Rockwell Hardness Measurement of Metallic Materials. In *NIST Recommended Practice Guide*; Volume Special Publication 960-5; National Institute of Standards and Technology: Gaithersburg, MD, USA, 2001.

19.   Roos, E.; Maile, K.; Seidenfuß, M. *Werkstoffkunde für Ingenieure—Grundlagen, Anwendung, Prüfung*, 6th ed.; Springer: Berlin/Heidelberg, Germany, 2017.

20.   Charles, A.; Elkaseera, A.; Paggi, U.; Thijs, L.; Hagenmeyer, V.; Scholz, S. Down-facing surfaces in laser powder bed fusion of Ti6Al4V: Effect of dross formation on dimensional accuracy and surface texture. *Addit. Manuf.* **2021**, *46*, 102148. [CrossRef]

21.   Charles, A.; Bayat, M.; Elkaseer, A.; Thijs, L.; Hattel, J.H.; Scholz, S. Elucidation of dross formation in laser powder bed fusion at down-facing surfaces: Phenomenon-oriented multiphysics simulation and experimental validation. *Addit. Manuf.* **2022**, *50*, 102551. [CrossRef]